Bond- versus site-centred ordering and possible ferroelectricity in manganites

DMITRY V. EFREMOV[1], JEROEN VAN DEN BRINK[2]* AND DANIEL I. KHOMSKII[1,3]

[1]Laboratory of Solid State Physics, Material Science Center, University of Groningen, Nijenborgh 4, 9747 AG Groningen, The Netherlands
[2]Instituut-Lorentz for Theoretical Physics, Leiden University, PO Box 9506, 2300 RA Leiden, The Netherlands
[3]II Physicalisches Institut, Universität zu Köln, Zuelpicher Strasse 77, 50937 Köln, Germany
*e-mail: brink@ilorentz.org

Published online: 21 November 2004; doi:10.1038/nmat1236

Transition metal oxides with a perovskite-type structure constitute a large group of compounds with interesting properties. Among them are materials such as the prototypical ferroelectric system $BaTiO_3$, colossal magnetoresistance manganites and the high-T_c superconductors. Hundreds of these compounds are magnetic[1], and hundreds of others are ferroelectric[2], but these properties very seldom coexist. Compounds with an interdependence of magnetism and ferroelectricity could be very useful: they would open up a plethora of new applications, such as switching of magnetic memory elements by electric fields. Here, we report on a possible way to avoid this incompatibility, and show that in charge-ordered and orbitally ordered perovskites it is possible to make use of the coupling between magnetic and charge ordering to obtain ferroelectric magnets. In particular, in manganites that are less than half doped there is a type of charge ordering that is intermediate between site-centred and bond-centred. Such a state breaks inversion symmetry and is predicted to be magnetic and ferroelectric.

Perovskites consist of corner-sharing O_6 octahedra with a transition metal ion in the centre. Almost all the ferroelectric perovskites contain non-magnetic transition metal ions with an empty *d*-shell (d^0 configuration), for example Ti^{4+}, Nb^{5+} and W^{6+}. Apparently the presence of the d^0 plays an important role in formation of a ferroelectric state[3,4]. In all of these systems ferroelectricity originates from a shift of the transition metal ion from the centre of the O_6 octahedron. In this way a stronger covalent bond with one (or three) instead of six weaker bonds with neighbouring oxygen atoms is formed[5].

The problem of why magnetism and ferroelectricity seem to be mutually exclusive has received some attention[3,4]. The most plausible explanation has to do with the Hund's rule coupling that tends to keep the spins of the open transition metal 3*d* shell in parallel orientation. This mechanism breaks the strong covalent bonds that are necessary for ferroelectricity. Thus this makes the usual stabilizing mechanism for ferroelectricity, related to the shift of transition metal ions, ineffective[3].

There are apparently three exceptions to the empirical assertion of the incompatibility of magnetism and ferroelectricity in perovskites: $BiFeO_3$, $BiMnO_3$ and $RMnO_3$ (R = Y or another small rare-earth ion). But actually even these compounds are not exceptions to the general rule, as the mechanism of ferroelectricity here is different from the conventional one. In $BiFeO_3$ and in $BiMnO_3$ ferroelectricity is due to the lone pairs of non-magnetic[6] Bi, and in $YMnO_3$ it is due to tilting of almost rigid MnO_5 trigonal bipyramids[7]. This last example shows that the shift of the transition metal ion from the centre of the O_6 octahedron is not the only feasible mechanism of ferroelectricity. Recently ferroelectricity was observed in $TbMnO_3$, and was attributed to magnetic frustration in this system[8]; a similar mechanism seems to operate[9] in $TbMn_2O_5$. Here we present a mechanism for the creation of ferroelectricity that is based on the interplay of magnetic, charge and orbital ordering in doped transition metal oxides, and in particular in manganites.

We consider doped manganites of the type $R_{1-x}Ca_xMnO_3$, with R = La, Pr. Different types of magnetic, charge and orbital orderings are observed in this class of compounds. It becomes more and more clear (see for example, ref. 10) that the charge and orbital

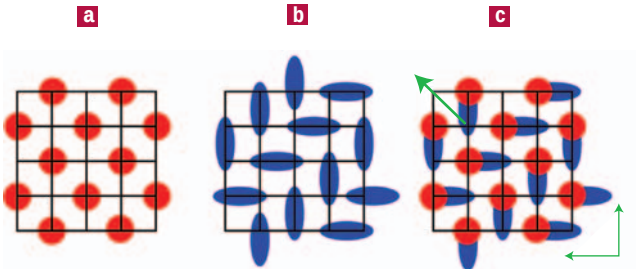

Figure 1 **Three types of charge ordering. a**, Site-centred charge order; **b**, bond-centred charge order (the Zener polaron state); and **c**, a ferroelectric intermediate state. The charge-ordered structure in **c** lacks inversion symmetry. Thin green arrows indicate the dipole moments of horizontal and vertical dimers, and the diagonal arrow is the total ferroelectric moment.

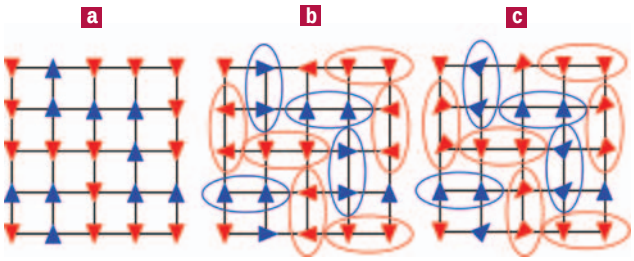

Figure 2 **Concomitant magnetic order of the three charge-ordered phases in Fig. 1. a**, The magnetic CE-phase ($\Phi = 0$); **b**, the orthogonal magnetic phase ($\Phi = \pi/2$); and **c**, the magnetic structure of a ferroelectric intermediate state $I(\Phi)$ (where $0 < \Phi < \pi/2$).

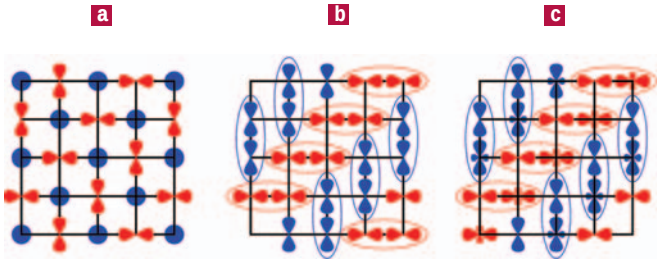

Figure 3 **Schematic representation of the orbital order in the three charge-ordered phases. a**, Site-centred ordering; **b**, bond-centred ordering; and **c**, the ferroelectric intermediate state.

superstructures existing in them are different from the usually assumed ordering of well-localized ionic states of Mn, and rather have the nature of charge/orbital density waves. This modifies the description of these orderings, and, as we show below, leads to new phenomena—one possibility being ferroelectricity.

We focus our attention to doping concentrations close to $x \approx 0.5$ (where there is one extra electron per two Mn ions). In the La–Ca system charge ordering exists for $x \geq 0.5$, and in the Pr–Ca system charge ordering extends down to $x \approx 0.3$. It is widely believed that the charge-ordering pattern in these compounds is of a simple checkerboard type[11–15]; see Fig. 1a. The checkerboard pattern is characterized by the alternation of Mn^{3+} and Mn^{4+} sites (although in practice the degree of charge disproportionation is usually less, never reaching the pure 3+/4+ valence states). We refer to such a pattern as Mn-centred (in general metal-, or site-centred) charge ordering (SCO).

However, in principle another charge-ordering pattern may exist, where the charge is localized not on sites but on bonds. In this situation the metal sites remain equivalent. Such a bond-centred charge ordering (BCO) is very well known in low-dimensional (mostly organic) compounds, where it is known as the Peierls distorted state. But only recently the first experimental observation of a BCO in three-dimensional transition metal oxides has been reported[16]: the system $Pr_{1-x}Ca_xMnO_3$ with $x \approx 0.4$ was shown to have a bond-centred charge-ordering pattern, of a type shown in Fig. 1b. Recently the BCO state has also been found theoretically in Hartree–Fock calculations of the electronic structure and in a phenomenological symmetry classification scheme[17–19]. The presence of a BCO demands a marked change in our understanding of charge ordering, and not only for manganites. It may imply that in all cases of charge order in oxides one should have in mind, besides the usual site-centred charge order, alternative states with bond-centred superstructures.

How can a BCO state appear at around $x \approx 0.4$ and a SCO around $x \approx 0.5$? We address this question by using the model and approach suggested previously[20], which proceeds from a more itinerant description of e_g electrons and which is a generalization of the magnetic double-exchange model[21] to the case of degenerate orbitals ('degenerate double exchange', DDEX). In this model, magnetic, orbital and charge-ordering structures are closely related to each other. The model does not take into account some factors, for example the role of disorder, which may be important for certain properties of real manganites. It does, however, contain the physics of the main effects that we discuss here. DDEX has proved to be very successful in explaining the magnetic, orbital and charge-ordering properties of over-doped[20] and half-doped[22] manganites. We used this method to check the stability of SCO relative to BCO, and indeed observed a finite range of existence for both.

The unexpected outcome of our study is that, besides these two pure states, we obtain an intermediate phase that combines both these features. The charge-ordering pattern of such an intermediate state is indicated in Fig. 1c. From the figure it is immediately clear that the charge-ordering pattern of this state lacks inversion symmetry and is ferroelectric. According to DDEX, this ferroelectricity should be intimately connected to the magnetic order.

In DDEX the localized spins (in manganites the spins of t_{2g} electrons) interact through the strong ferromagnetic Hund's rule coupling with the itinerant electrons moving in the valence bands formed by the degenerate e_g levels. Localized spins on neighbouring sites interact through an antiferromagnetic exchange. For strong Hund's rule coupling only those states with the spin of the e_g electron parallel to the localized spins are allowed, and we get the standard double-exchange model, generalized to the situation with degenerate conduction electrons. The DDEX Hamiltonian is[20]

$$H_{\mathrm{DDEX}} = \Sigma_{<ij>} t_{ij} \Gamma_{ij}^{\alpha\beta} c_{i\alpha}^{+} c_{j\beta} + J \Sigma_{<ij>} \mathbf{S}_i \cdot \mathbf{S}_j,$$

where the sum is over nearest neighbours and the first term describes the motion of the conduction electrons in the degenerate e_g bands α and β. The e_g hopping integral is t_{ij} and $\Gamma_{ij}^{\alpha\beta}$ is the e_g symmetry factor that depends on orbital index (α,β) and the direction of the lattice vector connecting neighbouring sites i and j in the lattice. The orbitals of e_g symmetry are $x^2 - y^2$ and $3z^2 - r^2$ (abbreviated as z^2). The symmetry factors are then

$$\Gamma_{\langle ij\rangle//z}^{z^2,\,z^2} = 1, \quad \Gamma_{\langle ij\rangle//x}^{z^2,\,z^2} = \tfrac{1}{4}$$

and

$$\Gamma_{\langle ij\rangle//x}^{x^2-y^2,\,x^2-y^2} = \tfrac{3}{4}.$$

Besides this, there is the usual dependence of hopping on the angle θ_{ij} between neighbouring spins: $t_{ij} = t\cos\theta_{ij}/2$. The strength of the antiferromagnetic exchange is determined by J and the superexchange energy per bond is $J\mathbf{S}\cdot\mathbf{S} = J\mathbf{S}^2\cos\theta_{ij}$.

We calculate the ground-state energy for different magnetic states. For each particular magnetic structure we determine the orbital and charge-ordering pattern. Besides considering the simple ferromagnetic (F) or antiferromagnetic (G) orderings, we also treat the somewhat more complicated A-, C- and CE-type antiferromagnetic states. These phases correspond to ferromagnetic planes coupled antiferromagnetically, ferromagnetic chains coupled antiferromagnetically and ferromagnetic zigzag chains coupled antiferromagnetically, respectively. The latter CE phase is shown in Fig. 2a.

In addition to these common magnetic orderings we also examine two new magnetic phases. The basic building blocks

of these magnetic structures, which we refer to as the ⊥ and 120° phase, are dimers. We consider coverage of the lattice by dimers as shown in Fig. 2b. Because of the double exchange process, spins within a dimer are aligned ferromagnetically; they are called Zener polarons. One can show that the total spins of two neighbouring dimers that are parallel to the same crystallographic direction are aligned antiferromagnetically. Neighbouring horizontal and vertical dimers have in general non-collinear spins. One such state is the perpendicular (⊥) spin structure of Fig. 2b; this is the optimal magnetic ordering for the Zener polaron state of ref. 16. In the 120° phase, the spins of dimers form three sublattices with angles of 120° between them (the best classical ordering in a triangular lattice of dimers).

It is possible to go from the CE ordering of Fig. 2a to the ⊥ phase of Fig. 2b by a continuous rotation of dimer spins (see Fig. 2c). All the magnetic states that are intermediate between CE and ⊥ are allowed by symmetry. Every such intermediate state, which we denote as $I(\Phi)$, is characterized by an angle Φ, where the extreme $\Phi = 0$ corresponds to the CE phase and the extreme $\Phi = \pi/2$ corresponds to the ⊥ phase.

The calculated phase diagram as a function of doping x and dimensionless coupling J/t is shown in Fig. 4. We focus on the region of stability of the intermediate phase $I(\Phi)$, denoted FE in Fig. 4a. For physical values of J/t, the intermediate phase is stable from about $x = 0.4$ to $x = 0.5$. At around $x = 0.4$ we find that $\Phi = \pi/2$, corresponding to the ⊥ phase. With increasing x, Φ gradually decreases until $x = 0.5$, where we reach $\Phi = 0$ (corresponding to the CE phase); see Fig. 4. Only at the phase boundaries are the pure CE and ⊥ phases stable. Indeed, experimentally, the Zener polaron phase is reported for doping concentrations of[16] $x \approx 0.4$ and the CE phase[11–15] for $x = 0.5$.

To understand why the intermediate phase $I(\Phi)$ is stable, we need to know why the two extremes $\Phi = 0$ (CE phase) and $\Phi = \pi/2$ (⊥ phase) are stable ground states. It is well known that the stability of the CE phase is due to the ordering of the orbital degrees of freedom[11–15]. Here we argue that the same holds for the ⊥ phase and thus for the entire intermediate phase $I(\Phi)$; for more details see the Methods section.

The ordering considered above corresponds to an experimental situation in which the main charge and orbital superstructure is commensurate with the lattice. An example would be Pr–Ca manganites with values of x from about 0.3 to 0.5. For $x > 0.5$ the superstructure in manganites is usually incommensurate. The reason for such different behaviour is not clear at present. Here we restrict ourselves to doping concentrations $x < 0.5$ with the commensurate superstructure.

Our intermediate phase $I(\Phi)$ is charge- and orbital-ordered for all values of Φ. The calculated ordering patterns as a function of doping concentration are schematically indicated in Figs 1 and 3. Charge ordering is driven by the inter-site Coulomb interaction and also by Coulomb interaction U between electrons on the same site[17]. We calculate the latter effect within a straightforward Hartree–Fock approach. We do indeed find a charge-ordering pattern that is in-between SCO and BCO (Fig. 1c). The calculated valence difference between the two Mn ions in a dimer Δq is no larger than $0.1e$ (see Fig. 4). Within a dimer the inversion symmetry is broken and each dimer attains a dipole moment. All these moments together add up to a net polarization of each plane. As the neighbouring planes order in phase[11–16], this leads to a ferroelectric state of the whole crystal. This important result does not depend on the details of the model that we used for our calculations. It is the underlying symmetry that leads to a ferroelectric charge-ordered state that lies between the extremes of the SCO and the BCO state. The observed symmetry of the novel phase in $Pr_{0.6}Ca_{0.4}MnO_3$ is[16] $P11m$: that is, it is indeed non-centrocymmetric. We conclude that these manganites

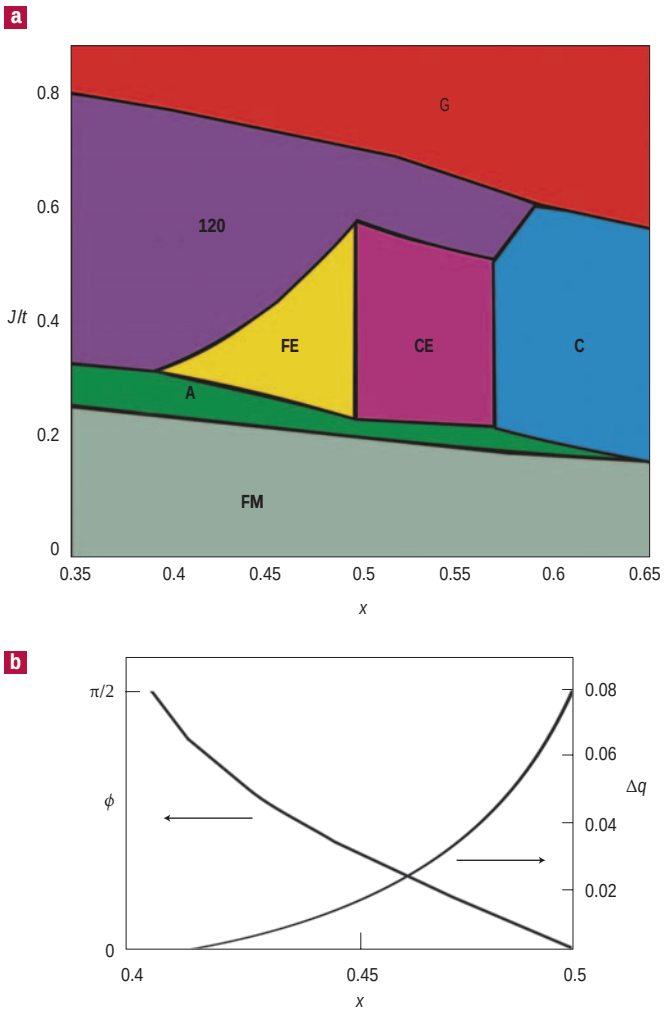

Figure 4 **Different phases and charge disproportionation in manganites for doping concentrations x around 0.5.** **a**, Phase diagram (see text for the various structures). The 120° phase corresponds to a Jaffet–Kittel-type magnetic ordering. The intermediate ferroelectric phase $I(\Phi)$ is coloured yellow. **b**, The value of the angle Φ in the intermediate phase and its charge disproportionation Δq (for Coulomb interaction U equal to the hopping matrix element t).

can be viewed as examples *par excellence* of magnetic systems that can become ferroelectric through the interplay of orbital ordering, charge ordering and magnetism.

One can estimate the values of the spontaneous polarization using the charge redistribution calculated above and taking the experimentally measured difference of the Mn–Mn distances within and between dimers[16]. From these values we get a net polarization per unit volume which is of the order of 1 mC m^{-2}, comparable in magnitude[8] to $TbMnO_3$, but much smaller than in classical ferroelectrics such as $BaTiO_3$. The switching of polarization (which is a requirement for real ferroelectrics) is achieved easily in our model, more easily than, for example, in $BaTiO_3$, as it requires predominantly a shift of electron charges from one end of a dimer to the other (with eventual shifts of intermediate oxygens), instead of the shift of heavy Ti ions in $BaTiO_3$.

Some measurements of the dielectric constant ε do show a peak in $\varepsilon(T)$ at the charge-ordering temperature in manganites[23] (see also ref. 24) which may be indicative of the ferroelectric phase that we

predict here. But one has to be careful because such measurements may be obscured by a finite conductivity: unfortunately the existing samples are not very good insulators.

It turns out, then, that the conventional picture of charge ordering as an ordered arrangement of Mn^{3+} and Mn^{4+} ions is oversimplified and, strictly speaking, incorrect: the actual ordering is closer to charge and orbital density waves. Our approach, proceeding from the double-exchange framework and taking into account orbital degeneracy, reproduces both the site-centred orbital ordering (for example, of conventional checkerboard type) and the bond-centred ordering ('Zener polarons'). Such charge-ordering patterns are not restricted to manganites alone, and probably occur also in other oxides. The most interesting result is that these two types of ordering may coexist, and the resulting state turns out to be ferroelectric. This novel mechanism of ferroelectricity opens yet another route to overcome the apparent incompatibility of ferroelectric and magnetic ordering in perovskites.

METHODS

The explanation for the stability of the intermediate phase $I(\Phi)$ can be obtained from our method used to calculate the phase diagram. Denote the general orbital state of a Mn ion as $|\gamma\rangle = \cos(\gamma/2)\,|z^2\rangle + \sin(\gamma/2)\,|x^2-y^2\rangle$ and first consider the orbital configuration of an isolated dimer made out of two Mn ions with one e_g-electron. In separate dimers that point along the crystallographic x-direction ('x-dimer') we have, for both sites in the dimer, $\gamma = 2\pi/3$. This corresponds to occupied $|x^2\rangle = |3x^2-r^2\rangle$ orbitals on both sites (see Fig. 3b). For an isolated dimer along the y-direction ('y-dimer') we have instead $\gamma = -2\pi/3$, corresponding to occupied $|y^2\rangle = |3y^2-r^2\rangle$ orbitals.

From our calculations of the extended system we know the wavefunctions and thus the orbital occupation on every site. For the $\perp$ phase, where there is hopping between neighbouring dimers, we find for the x-dimer that $\gamma \approx 130°$, which is mainly a $|x^2\rangle$ state, almost the same as for a non-interaction dimer, with a small admixture of the $|x^2-y^2\rangle$. Accordingly, for the y-dimer we find $\gamma \approx -130°$, which corresponds to a predominantly $|y^2\rangle$ state with some $|x^2-y^2\rangle$ character admixed. This admixture, although not large, is important because it is actually driving the stability of the $\perp$ phase. The superexchange tends to align the spins of neighbouring x- and y-dimers antiparallel. But in the $\perp$ phase these spins are only orthogonal, so that hopping between the dimers is possible, although reduced by a factor $1/\sqrt{2}$ from its maximum value. From this hopping between neighbouring dimers, which leads to the admixture of $|x^2-y^2\rangle$ states into the ground-state wavefunction, the system gains kinetic energy. The hopping amplitude between $|x^2\rangle$ orbitals of two neighbouring x-dimers (or between $|y^2\rangle$ orbitals of two neighbouring y-dimers) is much smaller, so that the spins of neighbouring dimers of the same kind tend to align themselves fully antiparallel. We conclude that the stability of the $\perp$ state, and thus of intermediate phase $I(\Phi)$, is caused by its orbital order which allows for an optimal compromise between electron delocalization (causing ferromagnetic double exchange) and antiferromagnetic superexchange interactions.

Received 3 June 2004; accepted 27 August 2004; published 21 November 2004.

References

1. Goodenough, J. B. & Longo, J. M. *Landolt-Boernstein, Numerical Data and Functional Relationships in Science and Technology* New Series Vol. III.4, 126 (Springer, Berlin, 1970).
2. Adachi, M. *et al. Landolt-Boernstein, Numerical Data and Functional Relationships in Science and Technology* New Series Vol. 16, 45 (Springer, Berlin, 1970).
3. Khomskii, D. I. Magnetism and ferroelectricity: why do they so seldom coexist? *Bull. Am. Phys. Soc.* C21.002 (2001).
4. Hill, N. A. Density functional studies of multiferroic magnetoelectric. *Annu. Rev. Mater. Res.* **32,** 1–37 (2002).
5. Cohen, R. E. Origin of ferroelectricity in oxide ferroelectrics and the difference in ferroelectric behavior of $BaTiO_3$ and $PbTiO_3$. *Nature* **358,** 136–138 (1992).
6. Seshadri, R. & Hill, N. A. Visualizing the role of Bi 6s 'lone pairs' in the off-center distortion in ferromagnetic $BiMnO_3$. *Chem. Mater.* **13,** 1892–2899 (2001).
7. van Aken, B. B., Palstra, T. T. M., Filippetti, A. & Spaldin, N. A. The origin of ferroelectricity in magnetoelectric $YMnO_3$. *Nature Mater.* **3,** 164–170 (2004).
8. Kimura, T. *et al.* Magnetic control of ferroelectric polarization. *Nature* **426,** 55–58 (2003).
9. Hur, N. *et al.* Electric polarization reversal and memory in a multiferroic material induced by magnetic field. *Nature* **429,** 392–394 (2004).
10. Loudon, J. C. *et al.* Weak charge-lattice coupling requires reinterpretation of stripes of charge order in $(La,Ca)MnO_3$. cond-mat/0308581 (2003).
11. Wollan, E. O. & Koeler, W. C. Neutron diffraction study of the magnetic properties of the series of perovskite-type compounds $La_{(1-x)}Ca_xMnO_3$. *Phys. Rev.* **100,** 545–563 (1955).
12. Goodenough, J. B. Theory of the role of covalence in the perovskite-type manganites La, M(II). MnO_3. *Phys. Rev.* **100,** 564–573 (1955).
13. Jirak, Z. *et al.* Neutron diffraction study of $Pr_{1-x}Ca_xMnO_3$ perovskites. *J. Magn. Magn. Mater.* **53,** 153–166 (1985).
14. Radaelli, P. G. *et al.* Charge, orbital, and magnetic ordering in $La_{0.5}Ca_{0.5}MnO_3$. *Phys. Rev. B* **55,** 3015–3023 (1997).
15. Grenier, S. *et al.* Resonant x-ray diffraction of the magnetoresistant perovskite $Pr_{0.6}Ca_{0.4}MnO_3$. *Phys. Rev. B* **69,** 134419 (2004).
16. Daoud-Aladine, A., Rodriguez-Carvajal, J., Pinsard-Gaudart, L., Fernandez-Diaz, M. T. & Revcolevschi, A. Zener polarons in half-doped manganites. *Phys. Rev. Lett.* **89,** 97205 (2002).
17. Ferrari, V., Towler, M. & Littlewood, P. B. Oxygen stripes in $La_{0.5}Ca_{0.5}MnO_3$ from ab initio calculations. *Phys. Rev. Lett.* **91,** 227202 (2003).
18. Zheng, G. & Patterson, C. H. Ferromagnetic polarons in $La_{0.5}Ca_{0.5}MnO_3$ and $La_{0.33}Ca_{0.67}MnO_3$. *Phys. Rev. B* **67,** 220404 (2003).
19. Shakhmatov, V. S., Plakida, N. M. & Tonchev, N. S. Orbital phase transition in $Pr_{1-x}Ca_xMnO_3$. *JETP Lett.* **77,** 18 (2003).
20. van den Brink, J. & Khomskii, D. Double exchange via degenerate orbitals, *Phys. Rev. Lett.* **82,** 1016–1019 (1999).
21. de Gennes, P. G. Effects of double exchange in magnetic crystals. *Phys. Rev.* **118,** 141–154 (1960).
22. van den Brink, J., Khaliullin, G. & Khomskii, D. Charge and orbital order in half-doped manganites. *Phys. Rev. Lett.* **83,** 5118–5121 (1999).
23. Jardon, C. *et al.* Experimental study of charge ordering transition in $Pr_{0.67}Ca_{0.33}MnO_3$. *J. Magn. Magn. Mater.* **196,** 475 (1999).
24. Mercone, S. *et al.* Anomaly in the dielectric response at the charge orbital ordering transition of crystalline $Pr_{0.67}Ca_{0.33}MnO_3$. *Phys. Rev. B* **69,** 174433 (2004).

Acknowledgements

We thank G. A. Sawatzky and J. Zaanen for discussions. This work was supported by the Stichting voor Fundamenteel Onderzoek der Materie (FOM), the Nederlandse organisatie voor Wetenschappelijk Onderzoek (NWO) and the Deutsche Forschungsgemeinschaft via SFB 608. Correspondence and requests for materials should be addressed to J.v.d.B.

Competing financial interests

The authors declare that they have no competing financial interests.